Available online at www.sciencedirect.com
ScienceDirect
Journal of Molecular Catalysis A: Chemical 271 (2007) 185–191
JOURNAL OF MOLECULAR CATALYSIS A: CHEMICAL
www.elsevier.com/locate/molcata

ONIOM study of Ga/SAPO-11 catalyst: Species formation and reactivity

Anibal Sierraalta [a,*], Rafael Añez [a], Elena Ehrmann [b]

[a] *Laboratorio de Química Computacional, Centro de Química, Instituto Venezolano de Investigaciones Científicas, Apartado 21827, Caracas 1020-A, Venezuela*
[b] *Departamento de, Procesos y Sistemas, Universidad Simón Bolívar, Valle de Sartenejas, Caracas, Venezuela*

Received 12 December 2006; received in revised form 27 February 2007; accepted 1 March 2007
Available online 6 March 2007

Abstract

In this study, we carried out two-layer ONIOM calculations to determine the Gibbs free energy and the enthalpy changes for the gallium-exchanged silicoaluminophospate (Ga/SAPO-11) catalysts' interaction with NH_3, SO_2, CH_3NH_2, CH_3SH, H_2, and H_2O molecules, and the formation of possible intermediate species, such as oxy-hydroxy $GaO_m(OH)_n$. The results reveal that the $[HGaOH]^+$ and $[Ga]^+$ formation, as well as the SO_2 adsorption at 773 K are thermodynamically favorable processes. This work shows for first time the potential ability of the Ga/SAPO-11 catalyst to adsorb SO_2 and to oxidize H_2S; that is, to be used in DeSOx reactions. NH_3 and CH_3NH_2 adsorption were also found to be exothermic processes, but thermodynamically favourable ($\Delta G < 0$) at temperatures below 773 K, whereas CH_3SH is not adsorbed at all. This implies that the Ga/SAPO-11 catalyst behaves like a hard acid according to Pearson's rule.

Keywords: ONIOM; Gallium catalysts; GaO; SAPO-11; DeSO*x*; Theoretical calculations; DFT; B3LYP

1. Introduction

Gallium based catalysts have been employed in several reaction types; for instance, Ga_2O_3/Al_2O_3 prepared via sol–gel methods has shown excellent activity for propane induced NO reduction in the presence of water [1]. Due to their good Lewis acidity, Ga catalysts have found application in the aldol-type reactions of silyl enol ethers with carbonyl compounds [2]. Ga-modified and Ga-exchanged zeolites have also been used for the alkylation of aromatic compounds [3], cycloalkane conversion [4], propane aromatization [5,6], selective catalytic NO reduction [7,8] More recently, the Ga/SAPO-11 system has been used for the direct transformation of *n*-butane to butenes [9].

In general, Ga-exchanged Zeolite catalysts are prepared by incipient wetness with Ga^{3+} salts [9–11] or by chemical vapor deposition of trimethylgallium [12,13] After impregnation, the solid is calcinated under dry air and reduced under H_2 atmosphere. EXASF and XANES techniques have shown that, after H_2 treatment, the Ga, originally deposited over the zeolite surface as Ga oxide (Ga_2O_3(s),) is reduced to Ga^{+1} [14–16] which reacts with the acidic sites of the support. Hensen et al. [11] demonstrated that Ga/ZSM-5 reduction with hydrogen at 773 K results in a complete substitution of the ZSM-5 acidic hydroxyl groups, according to the following net reaction:

$$Ga_2O_3(s) + 2(H^+Z^-) + 2H_2(g) \rightarrow 2(Ga^+Z^-) + 3H_2O \quad (1)$$

It is well known that H_2 reduction of Ga_2O_3(s) produces Ga_2O(g) [4,11,17] This gas migrates into the pores of the solid and reacts with the acid sites (H^+Z^-) of the support [5,6,10,11] to yield the Ga^+Z^- sites according to the following reactions:

$$Ga_2O_3(s) + 2H_2(g) \rightarrow Ga_2O(g) + 2H_2O \quad (2)$$

$$Ga_2O(g) + 2(H^+Z^-) \rightarrow 2(Ga^+Z^-) + H_2O \quad (3)$$

Several authors have studied the nature of the species present in the Ga/ZSM5 catalyst. Chao et al. [18] proposed that, after H_2 treatment, the Ga exists as some kind of Gallium hydride oligomer with bridging H atoms. Based on DRIFT spectroscopy [11] and in situ X-ray absorption [19] other authors concluded that the reduced Ga atoms are present as monomeric hydrides instead of oligomers, whereas a third group has suggested that these Gallium species are actually dihydrides [11,13,19].

* Corresponding author. Tel.: +58 212 5041774; fax: +58 212 5041350.
E-mail address: asierral@ivic.ve (A. Sierraalta).

1381-1169/$ – see front matter © 2007 Elsevier B.V. All rights reserved.
doi:10.1016/j.molcata.2007.03.002

Moreover, it has been proposed that these dihydride $[GaH_2]^+$ species constitute the catalytic sites for the dehydrogenation reactions [20–22]. Additionally, Védrine and co-workers [6] and Todorova and Su [23] proposed GaO(OH) and $Ga_2(OH)_xO_{3-x}$ as the forerunners of the $[Ga^+]$ and $[GaO]^+$ species.

Few studies have addressed the influence of the support on the activity of Ga catalysts. Machado et al. [9] studied the Ga/SAPO-11 system. Using H_2-TPR profiles, the authors concluded that the $[GaO]^+$ and $[Ga^+]$ cations could be the catalytic species responsible for the dehydrogenation of *n*-butane. Unfortunately, the experimental data was not conclusive. The aim of the present work is to aid in the understanding of the nature and the catalytic role of the possible extra-framework Ga species present in the Ga/SAPO-11 system. To achieve this objective, we performed a series of quantum chemical calculations for the $[GaO]^+$, Ga^+, $[HGaOH]^+$, and $[Ga(OH)_2]^+$ anchored species, as well as for the interaction of the gallilic ion with NH_3, SO_2, CH_3NH_2, CH_3SH probe molecules.

2. Models and methodology

The silicoaluminophospates molecular sieves (SAPO) are molecular structures that contain Si–O–Al, P–O–Al and Si–O–Si but no Si–O–P bonds. They have a medium pore structure with low density of moderate acid sites. The SAPO-11 principal channel contains rings of 10 tetrahedrons (T10.) The Brönsted acid sites of these structures are protons attached to the oxygen bridge of the Si–O–Al triads; mainly, inside the T10 rings [24,25]. The Si atoms are grouped into regions called *Si islands*. The Si atoms inside the *Si islands* are connected to each other by oxygens atoms; whereas at the island borders, the O bridges additionally connect Si to Al and Al to P. Scheme 1 displays a graphical representation of these island borders, where the O atoms bonded to Si and Al are identified as O_{Si} and the O atoms bonded to Al and P, as O_p. The basins created by this configuration constitute potential locations for the Ga atoms. Fig. 1 displays a perspective view of the location of the basins.

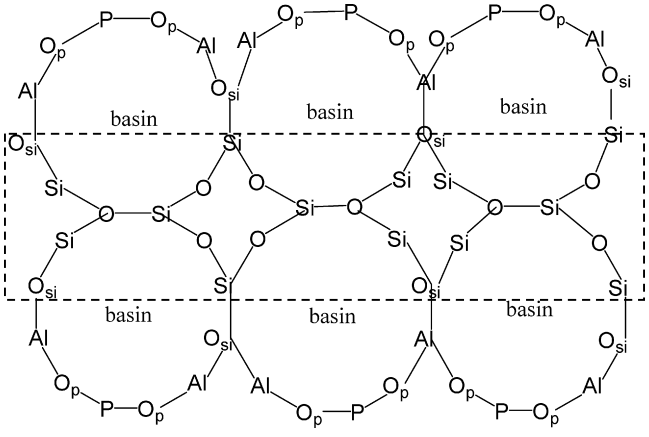

Scheme 1. Schematic representation of the basins into the SAPO-11 catalyst showing the Si islands, the O bridged atoms bonded to the Si and the Al atoms, O_{Si} atoms and the O bridged atoms bonded to the P and the Al atoms, O_P atoms. No all atoms are shown.

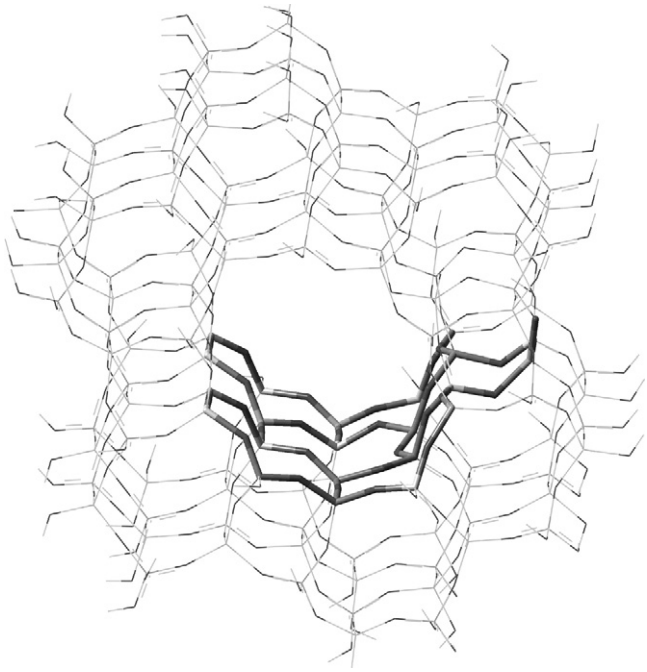

Fig. 1. View showing the relative position of the basins (tube) into the framework of the SAPO-11 (wireframe).

To model the SAPO-11, we employed a four layer structure, where each layer contains a T10 ring (4T10), as shown in Fig. 2a. This model comprises a total of 506 atoms. The SM2-SM3 rule [27,28], and results of previous calculations [26] were applied to localize the *Si islands* inside the 4T10 four layer model (see Fig. 2b).

Geometry optimizations, energy calculations and thermodynamic properties estimations were performed using the Gaussian-03 program [29]. The lower energy structures were obtained using the two-layer ONIOM methodology. Universal force field approach (UFF) was employed for the low level calculations and DFT approach (B3LYP) with the full-electron 3-21G* basis set for the high level. Thermodynamic properties were calculated at 773 K using only the high level model. This temperature was chosen because most experimental studies are performed at this value [9,11]. In general, the quality of the results using ONIOM is similar to those computed with periodic calculations [30] and with less computational cost, than did with comparable constrained clusters [31]. Beside this, it has been shown in the literature that the computed adsorption energies with ONIOM method compared well with experimentally reported values [32–34].

3. Results and discussions

3.1. On the thermodynamics of Ga species

In order to analyze the stability of the different Ga species possible, quantum chemical calculations were performed using the 4T10 model. Table 1 shows relevant geometrical properties and net charges for 4T10-Ga (Fig. 2), 4T10-GaO, 4T10-HGaOH (Fig. 3) and 4T10-$Ga(OH)_2$ (Fig. 4) species.

Table 1
Relevant bond distances (Å) and net charge for $[Ga]^+$ $[GaO]^+$, $[HGaOH]^+$ and $[Ga(OH)_2]^+$ species anchored in the 4T10 model

Structure	Relevant distances (Å)	Net charges[a]
4T10-Ga	Ga–Al = 3.31, Ga–Si = 3.08, Ga–O_{Si} = 2.14, Ga–O_P = 2.77	Q_{Ga} = +1.07
4T10-GaO	Ga–O = 1.71, Ga–Al = 3.16, Ga–Si = 2.88, Ga–O_{Si} = 1.97, Ga–O_P = 2.57	Q_{Ga} = +1.55, Q_O = −0.65
4T10-HGaOH	Ga–OH = 1.85, Ga–H = 1.57, Ga–Si = 2.93, Ga–Al = 3.31, Ga–O_P = 2.98, Ga–O_{Si} = 2.00	Q_{Ga} = +1.73, Q_{OH} = −0.58, Q_H = −0.32
4T10-$Ga(OH)_2$	Ga–OH = 1.84, Ga–Al = 3.28, Ga–Si = 2.88, Ga–O_{Si} = 1.98, Ga–O_P = 2.86	Q_{Ga} = +1.88, Q_{OH} = −0.55
4T10-$GaNH_3$	Ga–NH_3 = 2.39, Ga–Al = 3.48, Ga–Si = 3.04, Ga–O_{Si} = 2.41, Ga–O_P = 3.32	Q_{Ga} = +1.05, Q_{NH_3} = +0.08
4T10-$GaCH_3NH_2$	Ga–NH_2CH_3 = 2.33, Ga–Al = 3.28, Ga–Si = 3.13, Ga–O_{Si} = 2.30, Ga–O_P = 2.94	Q_{Ga} = +1.05, Q_{NH_3} = +0.09
4T10-GaO_2S	Ga–O_2S = 1.88, Ga–S = 2.61, Ga–Al = 3.23, Ga–Si = 2.82, Ga–O_{Si} = 1.94, Ga–O_P = 2.81	Q_{Ga} = +1.84, Q_{So_2} = −1.09

[a] APT net charge [35].

In general, the Ga–O_P bond distance is larger than the Ga–O_{Si} bond distance. Since P is more electronegative than Si, the bridging O atom of Al–O–P (O_P) has a more positive character than the one of Si–O–Al (O_{Si}). As a consequence, the gallilic ion is closer to the O_{Si} than to the O_P. Since the O_{Si} atoms are relatively close to each other and chemically similar, the Ga ion could potentially be located closer to one or the other O_{Si} atom inside the island basin. Indeed, quantum calculations corroborated that there exist two minimum energy positions for the gallilic ion inside the basin.

According to the results presented in Table 1, the Ga–O distance in 4T10-GaO is smaller than the corresponding Ga–O_P, Ga–O_{Si}, and Ga–OH distances. This ponts towards a higher bond index in the GaO moiety as compared to the other species; suggesting a double Ga–O bond. The Ga net charge in the 4T10-Ga structure is close to +1 (Q_{Ga} = +1.07); upon oxidation (4T10-GaO structure) as expected its charge increases from +1.07 to +1.55.

Frequency calculations for 4T10-HGaOH, and 4T10-$Ga(OH)_2$ models yield values of 3299 cm^{-1} and 3514 cm^{-1} for the OH stretching in 4T10-$Ga(OH)_2$ and 4T10-HGaOH, respectively. For the Ga–H in 4T10-HGaOH, a vibrational frequency value of 1966 cm^{-1} was obtained. The corresponding experimental values are 3672 cm^{-1} [13] and 3699 cm^{-1} [23] for GaOH, and 2040 and 2059 cm^{-1} [13], and 2020 cm^{-1} [36] for $[GaH]^+$. The differences between the calculated and the experimental vibrational frequency values lay within a ±200 cm^{-1} interval, which is acceptable considering the level of theory used in this work, and validate the model employed for the calculations.

Table 2 shows that the formation of the hydroxy as well as the dihydroxy species from $[Ga]^+$ (reactions 1 and 2, Table 2) or from $[GaO]^+$ with H_2O (reactions 3, Table 2) are energetically favorable processes. These results concur with calculations performed over a one tetrahedron structure by Chakraborty and co-workers [38]. It is noteworthy that our energy values are larger than those reported by Chakraborty due to the size of the model employed to represent the support and the level of theory used. The previous work [38] considered only one Al atom to represent the support, while the present work employed 24 atoms in the high level and 506 atoms in the low level for this purpose. The larger number of atoms in our model allowed the Ga atom to interact with more than two O atoms simultaneously. In fact, the minimum energy position corresponds to the Ga atom near the center of the basin (see Fig. 2). This type of geometry can not be obtained using models with only one Al atom. The

Table 2
Energy, reaction enthalpy and Free energy changes for some selected reactions, in kJ/mol

Reaction	ΔE	$\Delta H_{773\,K}$	$\Delta G_{773\,K}$
(1) 4T10-Ga + H_2O → 4T10-HGaOH	−143.6	−148.5	−62.1
(2) 4T10-Ga + $2H_2O$ → 4T10-$Ga(OH)_2$ + H_2	−343.3	−335.6	−198.9
(3) 4T10-GaO + H_2O → 4T10-$Ga(OH)_2$	−361.2	−349.2	−208.6
(4) 4T10-GaO + H_2 → 4T10-Ga + H_2O	−17.9	−13.6	−9.7
(5) 4T10-GaO + H_2 → 4T10-HGaOH	−161.5	−162.1	−71.7
(6) 4T10-HGaOH + H_2 → 4T10-GaH_2 + H_2O	+237.6	+235.1	+244.4
(7) 4T10-Ga + NH_3 → 4T10-$GaNH_3$	−139.2	−127.2	+11.7
(8a) 4T10-Ga + $2NH_3$ → 4T10-$Ga(NH_3)_2$	−106.8	–	–
(8b) 4T10-Ga + $2NH_3$ → 4T10-$Ga(NH_3)_2$	−84.6	–	–
(9) 4T10-Ga + CH_3NH_2 → 4T10-$GaNH_2CH_3$	−15.3	−63.2	+99.6
(10) 4T10-Ga + SO_2 → 4T10- GaO_2S	−207.3	−1224.9	−764.9
(11) 4T10-GaO_2S + $2H_2$ → 4T10-$Ga(OH)_2$ + H_2S	+28.5	+558.8	+301.1
(12) 4T10-Ga + SO_2 + $2H_2$ → 4T10-$Ga(OH)_2$ + H_2S	−178.9	−666.1	−463.8
(13) 4T10-GaO_2S + H_2 → 4T10-Ga(OH)(OSH)	−177.4	+363.3	+114.6
(14) 4T10-GaO_2S + H_2 → 4T10-$GaO(OSH_2)$	+97.2	+76.9	+184.4
(15) 4T10-Ga(OH)(OSH) + H_2 → 4T10-$Ga(OH)_2$ + H_2S	+205.9	+195.5	+186.5
(16) 4T10- $GaO(OSH_2)$ + H_2 → 4T10-$Ga(OH)_2$ + H_2S	−68.7	+481.9	+116.7

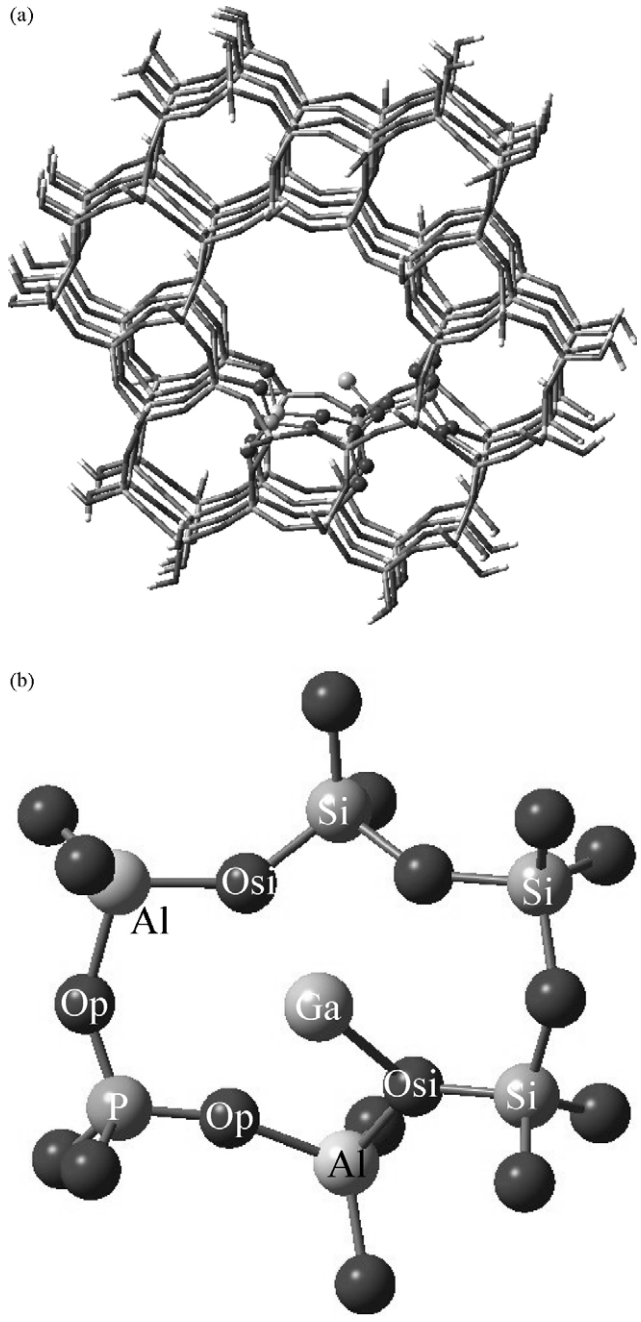

Fig. 2. (a) Molecular structure used to represent the Ga/SAPO-11 catalyst. The high level atoms are represented by spheres, the low level atoms by tubes. (b) Perpendicular near view of the basin with one Ga atom, showing the Ga, Osi, Op, Si, Al y P atoms.

Ga interaction with the atoms in the basin provides a greater stabilization energy for the Ga species. In agreement with the experimental evidence and previous calculations [26,38], the results of Table 2 show that the oxidized species $[GaO]^+$ can be reduced by H_2 to $[Ga]^+$ or $[HGaOH]^+$ (reactions 4 and 5). Accordingly, the inverse reaction; that is, the transformation of the hydroxy species into $[Ga]^+$ or $[GaO]^+$ is highly endothermic. This is consistent with the experimental fact that even after drying the Ga/ZSM5 at 873 K the signal that corresponds to the GaOH vibrational frequency remains present [6].

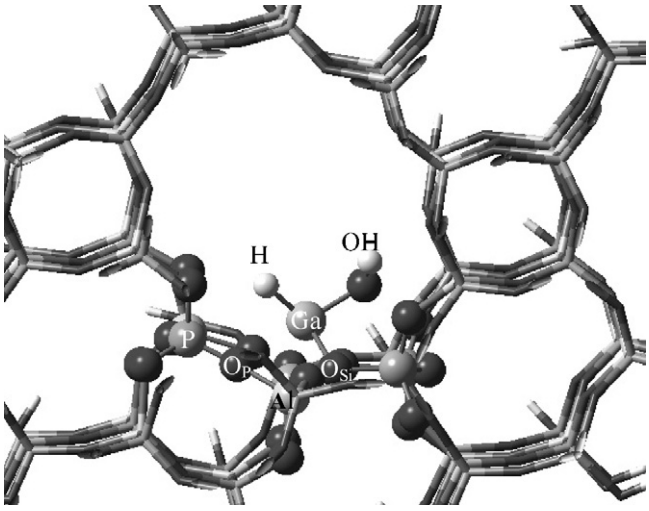

Fig. 3. Near view of the $[HGaOH]^+$ species in the 4T10-HGaOH model.

Reaction 8 of Table 2 shows that the reaction of the $[Ga]^+$ species with NH_3 is energetically favorable, which reveals a Lewis acid character for $[Ga]^+$. Moreover, the $[Ga]^+$ can interact simultaneously with two NH_3 molecules as shown in Table 2 (reactions 9a and 9b). However, the interaction with two NH_3 molecules is complex. The second NH_3 can (Fig. 5a) or not (Fig. 5b) interact with the first NH_3 and $[Ga]^+$ through the H bonds producing different type of complexes; as a consequence, different minima and interaction energy values are obtained (−106.8, −84.6 kJ/mol). The nature of the multiple NH_3 adsorption modes on Ga/SAPO-11 is beyond of the aim of this study and will not be further discussed.

Although energy change is a relevant reaction parameter, it is the thermodynamics that tells if the reaction proceeds spontaneously or not. It is well known that some exothermic reactions are not thermodynamically favorable. In order to investigate if the reactions studied herein are thermodynamically favorable or not, we performed ΔG and ΔH calculations at 773 K. Table 2 shows that the reductions of 4T10-GaO to yield either 4T10-Ga and water or 4T10-HGaOH (reactions 4 and 5, Table 2)

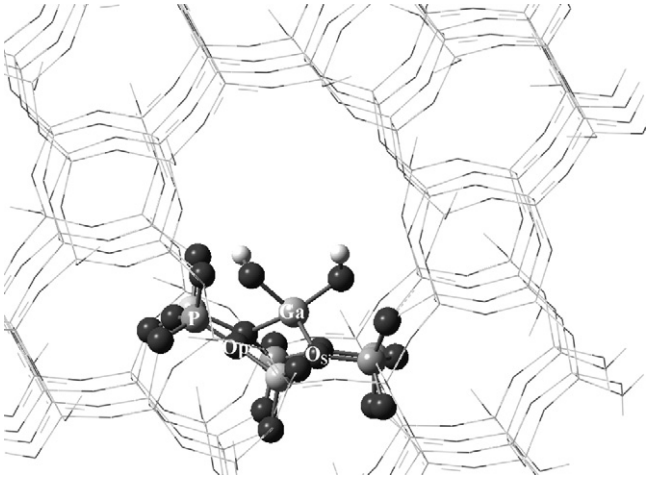

Fig. 4. Geometry of the $[Ga(OH)_2]^+$ species in the Ga/SAPO-11 catalyst according to the 4T10-$Ga(OH)_2$ model.

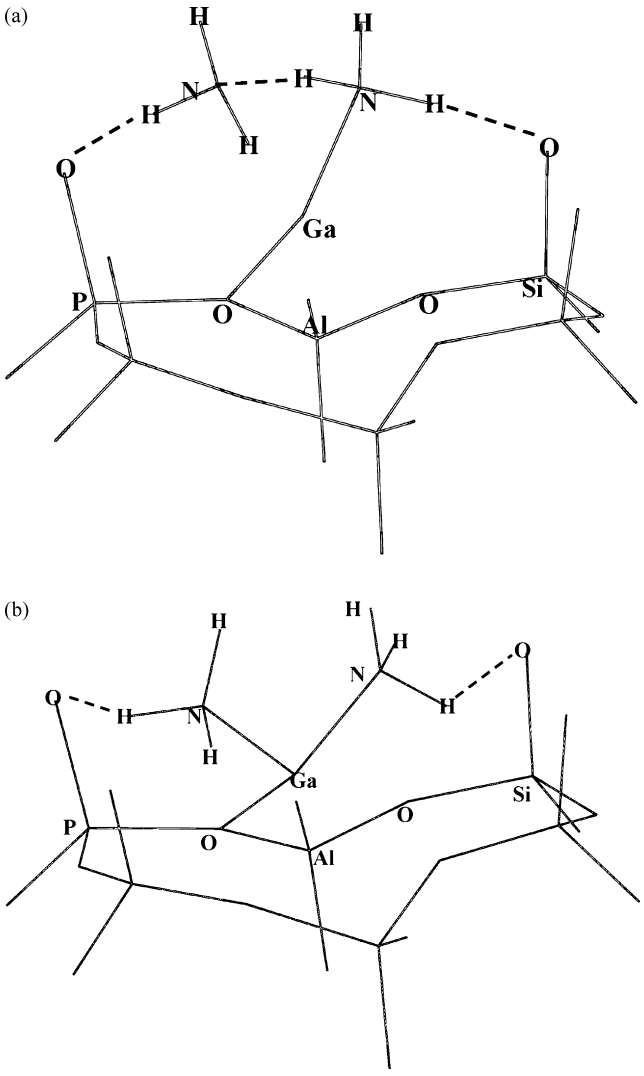

Fig. 5. (a) Schematic representation of the $[Ga(NH_3)_2]^+$ species 1 showing the interaction between the two NH_3 molecules through an H bond. Interaction energy −106.8 kJ/mol. (b) Schematic representation of the $[Ga(NH_3)_2]^+$ species 2 showing the interaction of the two NH_3 molecules with the Ga atom. Interaction energy −84.6 kJ/mol.

are spontaneous. According to Table 2 (reactions 1 and 2), the 4T10 exchanged Ga is susceptible to water, yielding the thermodynamically favorable $[HGaOH]^+$ and $[Ga(OH)_2]^+$ species Similarly, $[GaO]^+$ also forms the dihydroxy species upon reaction with water (reaction 3, Table 2). Even though the formation of $[HGaOH]^+$ from [GaO]+ is favored ($\Delta G = -71.7$ kJ/mol, reaction 5), further reduction of $[HGaOH]^+$ to form the dihydride species does not occur ($\Delta G = +244.4$ kJ/mol, reaction 7). These results are coherent with those reported by Kuzmin et al. [37] and Chakraborty and co-workers [38] for Ga/ZSM-5 catalysts; that is, $\Delta G = -347.7$ kJ/mol [37] and $\Delta G = -119.7$ kJ/mol [38] for the $[GaO]^+$/ZSM-5 reduction to $[HGaOH]^+$; and $\Delta G = +63.2$ kJ/mol for the $[HGaOH]^+$ reduction to $[GaH_2]^+$.

To determine whether Ga behaves as a hard or a soft acid in the Ga/SAPO-11 system, adsorption energies for NH_3, CH_3NH_2 and CH_3SH were calculated. The first two adsorbents are hard bases while the last one is a soft base. The results show that CH_3SH does not interact with the 4T10-Ga system while adsorption of NH_3 and CH_3NH_3 are thermodynamically favorable processes at certain temperatures. According to Table 2, $\Delta G = +11.7$ kJ/mol and $\Delta H = -127.2$ kJ/mol for NH_3 adsorption at 773 K (reaction 8). These values allowed to estimate that at T below 707 K (429 °C) ΔG is negative. Similarly for CH_3NH_3 adsorption, ΔG is negative at temperatures below 300 K. The previous results reveal that the Ga atom acts as a hard acid in the Ga/SAPO-11 system according to Pearson's empirical rule: *hard bases prefer hard acids and soft bases prefer soft acids*.

Calculations reveled a surprisingly strong interaction between 4T10-Ga and SO_2 (reaction 10, Table 2); that is, a highly exothermic SO_2 adsorption ($\Delta H = -1224.9$ kJ/mol) with a large negative ΔG value (−764.9 kJ/mol). This unexpected result opens the possibility that the Ga/SAPO-11 catalyst could be used as a DeSO*x* catalyst due to this highly favourable interaction with the SO_2 molecule. Even though the subsequent reduction of the $[GaO_2S]^+$ species with H_2 is not thermodynamically favored ($\Delta G = +301.1$ kJ/mol, reaction 11), the whole SO_2 to H_2S conversion processes is ($\Delta G = -463.8$ kJ/mol, reaction 12).

During SO_2 is adsorption, a net charge transfers occurs from the Ga atom to the SO_2, which indicates that the Ga atom is oxidized. The distance between Ga and the O atom of the SO_2 molecule (see Table 1, Fig. 6) is shorter that the corresponding $Ga–O_{Si}$ distance but similar to the Ga–OH distance, and larger than the Ga–O distance in the $[GaO]^+$ species (see Table 1, 4T10-GaO). These results point towards a Ga-O single bond formation at the expense of the S–O bond, which changes from 1.58 Å in the free SO_2 molecule to 1.72 Å in the adsorbed molecule.

The activation of the S–O bond suggests that the H_2S formation from $[GaO_2S]^+$ (Table 2, reaction 11) could proceed via a H_2 attack to this bond. This pathway, as well as the direct H_2 attack on the S atom were analyzed. Two stable intermediates were found. The first one results from the H_2 attack upon the S–O bond (Table 2, reaction 13, Fig. 7a) while second one results from the H_2 attack upon the S atom (Table 2, reaction

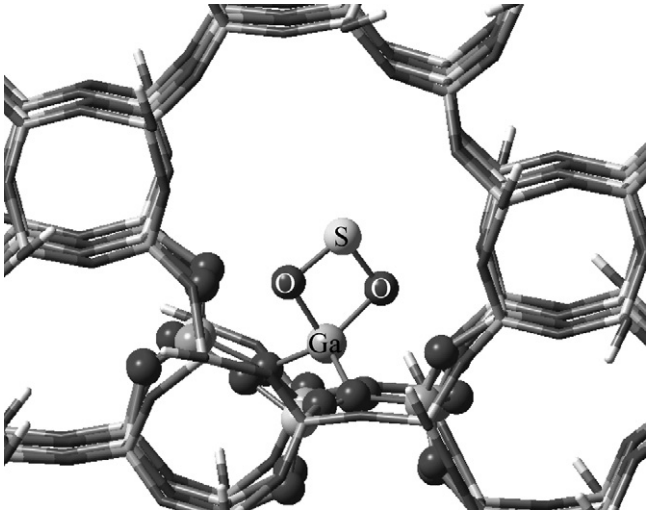

Fig. 6. Geometry of the $[GaO_2S]^+$ species in the Ga/SAPO-11 catalyst according to the 4T10-GaO_2S model.

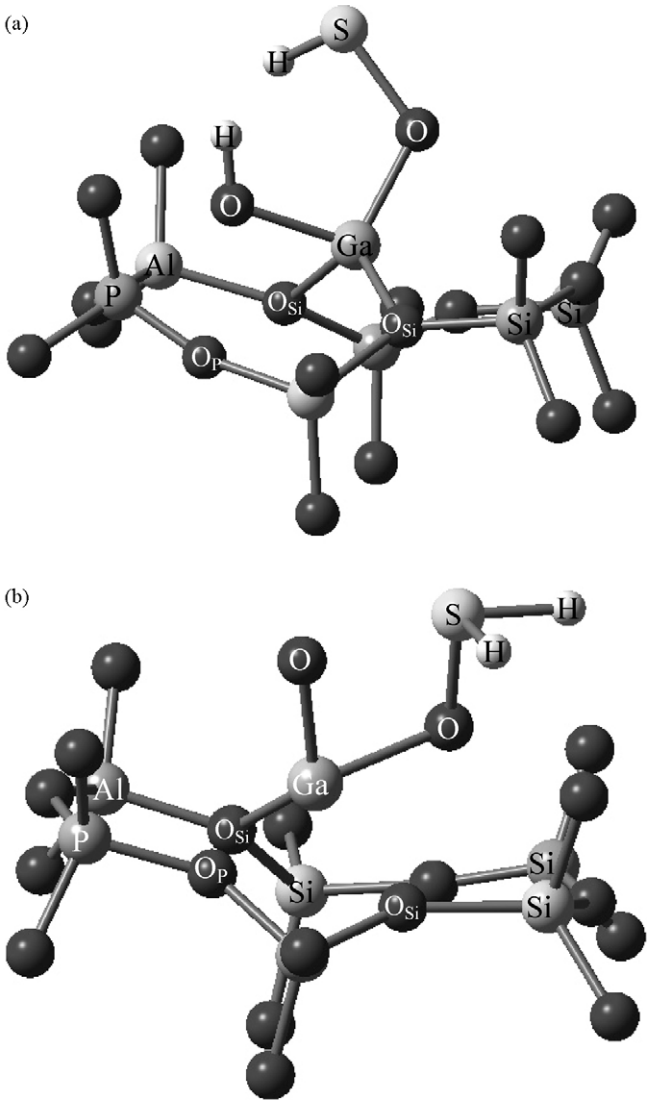

Fig. 7. (a) Geometry of the $[Ga(OH)(OSH)]^+$ species in the Ga/SAPO-11 catalyst according to the 4T10-Ga(OH)(OSH) model. (b) Geometry of the $[GaO(OSH_2)]^+$ species in the Ga/SAPO-11 catalyst according to the 4T10-$GaO(OSH_2)$ model.

14, Fig. 7b). According to the results, the H_2 attack upon the S–O bond produces the $[Ga(OH)(OSH)]^+$ intermediate, which is thermodynamically more stable than the one produced by the H_2 attack upon the S atom, $[GaO(OSH_2)]^+$. Therefore, considering the S–O activation and the $[Ga(OH)(OSH)]^+$ stability, it seems probable that the$[GaO_2S]^+$ reduction proceeds through a direct H_2 attack upon the S–O bond. It is worth noticing that the results of Table 2 show that the H_2S can be oxidized by the dihydroxy species, $[Ga(OH)_2]^+$ (reaction 11), to yield H_2 and $[GaO_2S]^+$ with a ΔG value of −301.1 kJ/mol. Thus, the quantum calculations show that the Ga/SAPO-11 system treated with H_2O could as well be a good solid for the H_2S elimination.

4. Conclusions

Minimum energy structures, thermodynamic properties and net charges for various Ga species supported on SAPO-11 were determined using *ab initio* calculations at density functional level. This work shows for the first time the potential use of Ga/SAPO-11 as a catalyst in DeSO*x* and H_2S elimination reactions. The calculation results reveal that: (1) the formation of the hydroxy species $[HGaOH]^+$ and $[Ga(OH)_2]^+$ from the reaction of $[Ga]^+$ or $[GaO]^+$ with H_2O is thermodynamically favorable. These species are quite stable even at 773 K. (2) The formation of $[GaH_2]^+$ from $[HGaOH]^+$ is not thermodynamically favorable; therefore, this species can not be considered as a forerunner for $[GaH_2^+]$. (3) The reduced Ga in the SAPO-11 behaves as a hard acid since it interacts with hard bases, such as NH_3, RNH_2, etc., but not with soft bases such as CH_3SH. (4) Supported Ga^+ interacts strongly with SO_2, which suggests that Ga/SAPO-11 catalysts could be candidates for DeSO*x* reactions. (5) The Ga dihydroxy species seems to be capable to oxidize $H_2S(g)$. Therefore, the hydroxylated Ga/SAPO-11 has potential as an $H_2S(g)$ elimination catalyst.

References

[1] M. Haneda, Y. Kintaichi, H. Shimada, H. Hamada, Chem. Lett. (1998) 181.
[2] H.-J. Li, H.-Y. Tian, Y.-J. Chen, D. Wang, C.-J. Li, Chem. Commun. (2002) 2994.
[3] C. Bigey, B.-L. Su, J. Mol. Catal. A: Chem. 209 (2004) 179.
[4] A. Raichle, S. Moser, Y. Traa, M. Hunger, J. Weitkamp, Catal. Commun. 2 (2001) 23.
[5] K. Nishi, S. Komai, K. Inagaki, A. Satsuma, T. Hatorri, Appl. Catal A: Gen. 223 (2002) 187.
[6] I. Nowak, J. Quartararo, E.G. Derouane, J.C. Védrine, Appl. Catal A: Gen. 251 (2003) 107.
[7] Y.J. Li, J.N. Armor, J. Catal. 145 (1994) 1.
[8] C. He, M. Paulus, J. Find, J.A. Nickl, H.-J. Eberle, J. Spengler, W. Chu, K. Köhler, J. Phys. Chem. B 109 (2005) 15906.
[9] F. Machado, C.M. Lopez, Y. Campos, A. Bolívar, S. Yunes, Appl. Catal. A: Gen. 226 (2002) 241.
[10] Y. Diaz, L. Melo, M. Mediavilla, A. Albornoz, J.L. Brito, J. Mol. Catal. A: Chem. 227 (2005) 7.
[11] V.B. Kazansky, I.R. Subbotina, R.A. van Santen, E.J.M. Hensen, J. Catal 227 (2004) 263.
[12] N. Rane, A.R. Overweg, V.B. Kazansky, R.A. van Santen, E.J.M. Hensen, J. Catal. 239 (2006) 478–485.
[13] V.B. Kazansky, I.R. Subbotina, R.A. van Santen, E.J.M. Hensen, J. Catal. 233 (2005) 351.
[14] A.C. Wei, P.H. Liu, K.J. Chao, E. Yang, H.Y. Cheng, Microporous Mesoporous Mater. 47 (2001) 147.
[15] G.L. Price, V. Kanazirev, J. Catal. 126 (1990) 267.
[16] R. Carli, C.L. Bianchi, R. Giannantonio, V. Ragaini, J. Mol. Catal. 83 (1993) 379.
[17] K. Nishi, S. Komai, K. Inagaki, A. Satsuma, T. Hattori, Appl. Catal. A: Gen. 223 (2002) 187.
[18] K.J. Chao, A.C. Wei, H.C. Wu, J.F. Lee, Microporous Mesoporous Mater. 35 (2002) 241.
[19] G.D. Meitzner, E. Iglesias, J.E. Baumgartner, E.S. Huang, J. Catal. 140 (1993) 209.
[20] M.S. Pereira, M.A.C. Nascimento, Chem. Phys. Lett. 406 (2005) 446.
[21] M.V. Frash, R.A. van Santen, J. Phys. Chem. A 104 (2000) 2468.
[22] Y.V. Joshi, K.T. Thomson, Catal. Today 105 (2005) 106.
[23] S. Todorova, B.-L. Su, J. Mol. Catal. A: Chem. 201 (2003) 223.
[24] Database of Zeolita Structure: http://www.iza-structure.org/databases.
[25] F. Salehirad, M.W. Anderson, J. Chem. Soc., Faraday Trans. 94 (1998) 2857.
[26] A. Sierraalta, Y. Guillen, C.M. Lopez, R. Marinez, F. Ruette, F. Machado, M. Rosa-Brussin, H. Soscun, J. Mol. Catal. A: Chem. 242 (2005) 233.

[27] F.J. Machado, C.M. Lopez, J. Goldwasser, B. Mendez, Y. Campos, D. Escalante, M. Tovar, Zeolitas 19 (1997) 387.
[28] G. Sastre, D.W. Lewis, C.R.A. Catlow, J. Mol. Catal. A: Chem. 119 (1997) 349.
[29] M.J. Frisch, G.W. Trucks, H.B. Schlegel, G.E. Scuseria, M.A. Robb, J.R. Cheeseman, J.A. Montgomery Jr., T. Vreven, K.N. Kudin, J.C. Burant, J.M. Millam, S.S. Iyengar, J. Tomasi, V. Barone, B. Mennucci, M. Cossi, G. Scalmani, N. Rega, G.A. Petersson, H. Nakatsuji, M. Hada, M. Ehara, K. Toyota, R. Fukuda, J. Hasegawa, M. Ishida, T. Nakajima, Y. Honda, O. Kitao, H. Nakai, M. Klene, X. Li, J.E. Knox, H.P. Hratchian, J.B. Cross, V. Bakken, C. Adamo, J. Jaramillo, R. Gomperts, R.E. Stratmann, O. Yazyev, A.J. Austin, R. Cammi, C. Pomelli, J.W. Ochterski, P.Y. Ayala, K. Morokuma, G.A. Voth, P. Salvador, J.J. Dannenberg, V.G. Zakrzewski, S. Dapprich, A.D. Daniels, M.C. Strain, O. Farkas, D.K. Malick, A.D. Rabuck, K. Raghavachari, J.B. Foresman, J.V. Ortiz, Q. Cui, A.G. Baboul, S. Clifford, J. Cioslowski, B.B. Stefanov, G. Liu, A. Liashenko, P. Piskorz, I. Komaromi, R.L. Martin, D.J. Fox, T. Keith, M.A. Al-Laham, C.Y. Peng, A. Nanayakkara, M. Challacombe, P.M.W. Gill, B. Johnson, W. Chen, M.W. Wong, C. Gonzalez, J.A. Pople, Gaussian 03, Revision D. 02, Gaussian, Inc., Wallingford, CT, 2004.
[30] X. Solans-Monfort, M. Sodupe, V. Branchadell, J. Sauer, R. Orlando, P. Ugliengo, J. Phys. Chem. B 109 (2005) 3539.
[31] J.T. Fermann, T. Moniz, O. Kiowski, T.J. McIntire, S.M. Auerbach, T. Vreven, M.J. Frisch, J. Chem. Theory Comput. 1 (2005) 1232.
[32] S. Namuangruk, P. Pantu, J. Limtrakul, J. Catal. 225 (2004) 523.
[33] S. Namuangruka, D. Tantanak, J. Limtrakul, J. Mol. Catal. A: Chem. 256 (2006) 113.
[34] J. Lomratsiri, M. Probst, J. Limtrakul, J. Mol. Graphics Modell. 25 (2006) 219.
[35] J. Cioslowski, J. Am. Chem. Soc. 111 (1989) 8333.
[36] S.E. Collins, M.A. Baltanas, J.G. Fierro, A. Bonivardi, J. Catal. 211 (2002) 252.
[37] I.V. Kuzmin, G.M. Zhidomirov, E.J.M. Hensen, Catal. Lett. 108 (2006) 187.
[38] N.O. Gonzales, A.K. Chakraborty, A.T. Bell, Top. Catal. 9 (1999) 207.